Optimizing IRS-Assisted Uplink NOMA System for Power Constrained IoT Networks

Mahmoud AlaaEldin*, Emad Alsusa*, Karim G. Seddik†, and Mohammad Al-Jarrah*

*Electrical and Electronic Engineering Department, University of Manchester, Manchester, UK M13 9PL
†Department of Electronics and Communications Engineering, American University in Cairo, Cairo, Egypt 11835

***Abstract*—This article presents a novel approach for power-constrained internet of things (IoT) networks that employ non-orthogonal multiple access (NOMA) and is assisted by an intelligent reflecting surface (IRS) for uplink transmissions. The main objective of this work is to maximize the sum rate of power-constrained IoT networks by jointly designing the IRS phase shifts and users' transmit power allocation. The proposed solution optimizes the power allocation and phase shifts alternatively. We devise a novel approach to optimize the IRS phase shifts that is based on manifold optimization techniques. Specifically, the IRS phase shifts optimization problem is formulated and solved over the complex circle manifold. Our results show that the proposed method outperforms the widely used semi-definite relaxation (SDR) method as higher sum rates with less power consumption can be achieved.**

I. Introduction

Energy efficiency is a key feature for the current and future generations of wireless networks, i.e., 5G and beyond, that enables the deployment of large-scale energy autonomous networks (EANs) [1], [2]. Moreover, the increasing demands on wireless sensor networks (WSNs), as an integral part of the emerging internet-of-things (IoT) technology, have raised the necessity of designing low energy consumption networks since wireless sensors generally have limited power resources [3], [4]. There is a wide range of applications for energy-autonomous wireless sensor networks (EAWSNs), including cellular networks in rural areas, e-farming, environmental monitoring, etc. [5], [6].

Furthermore, with the tremendous growth in the number of wireless devices connected to the cloud, such as smartphones, laptops, ipads, IoT devices, etc., with stringent quality-of-service (QoS) requirements, new telecommunication technologies and schemes have been developed to keep abreast of up-to-date requirements. The intelligent reflective surfaces (IRS) technology and non-orthogonal multiple access (NOMA) scheme are two of the most popular and widely accepted solutions in the literature for future wireless connectivity [7], [8]. IRSs have been introduced in the literature to control the wireless medium between transceivers by using a large number of reflectors that can apply phase shifts to the incident waves [9], [10]. In typical IRS-based wireless communications, the applied phase shifts are designed such that reflected signals add coherently at the receiver to improve the received signal-to-noise ratio (SNR) [11]–[13] . On the other hand, the spectral efficiency of wireless networks can be enhanced by employing NOMA, where several user equipments (UEs) are allowed to share the transmission medium simultaneously at the expense of some additional receiver circuitry for successive interference cancellation (SIC) implementation [14].

The integration between IRS technology and NOMA scheme has been considered in [15]–[17] to enhance the coverage and energy efficiency of the network downlink transmissions. The authors in [15] aim at maximizing the system energy efficiency by jointly optimizing the transmit beamforming at the base-station (BS) and the beamforming matrix at the IRS panel, where the optimization problem has been solved using alternating optimization (AO) technique with semi-definite relaxation (SDR). In [16], the beamforming vectors at the BS and the IRS phase shift matrix have been optimized to minimize the total transmission power where SDR and quadratic transform are exploited. The performance of multi-antenna IRS-NOMA networks is analyzed in [17] for both continuous and discrete IRS phase shifts scenarios. Moreover, the IRS-NOMA integration for uplink wireless communications is considered in [18]–[20]. The sum rate maximization for uplink IRS-NOMA is introduced in [18], where a joint users' power control mechanism and IRS beamforming problem is formulated and sub-optimally solved with the use of AO and SDR. In [19], IRS-NOMA for wireless power communications network (WPCN) is considered. Analysis for the outage probability of uplink IRS-NOMA is performed in [20].

As can be concluded from the discussions above, the synergy between IRS and NOMA solutions has merit for designing energy-efficient IoT networks. To the best of the authors' knowledge, the problem of maximizing the sum rate of IRS-NOMA for uplink transmissions using manifold optimization techniques has not been considered in the literature. Therefore, this paper provides such an approach and shows that manifold-based optimization provides superior performance compared to the widely adopted SDR [21]–[23]. Moreover, a comparison between IRS-NOMA and IRS-orthogonal multiple access (OMA) in terms of the achievable sum rate for a given power budget is provided. The optimal phase shifts at the IRS in the case of IRS-OMA are applied, whereas a suboptimal solution for IRS-NOMA is employed using AO supported by manifold optimization since the optimal solution is not tractable. The simulation results demonstrate that the proposed manifold optimization-based algorithm provides superior performance in the achievable sum rate compared to the conventional SDR technique. Additionally, the results reveal that IRS-NOMA can

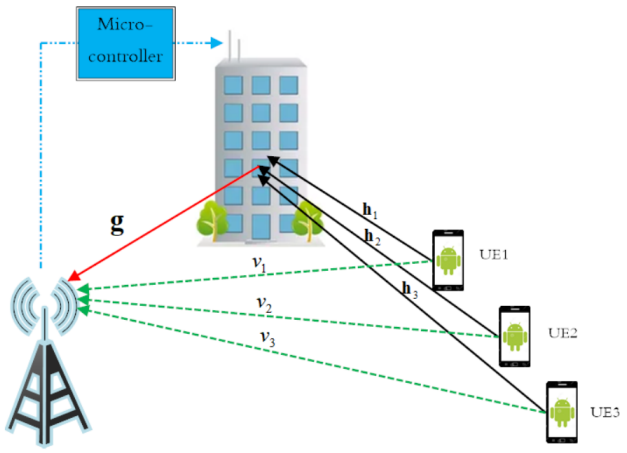

Figure 1: IRS-assisted NOMA uplink system model

achieve higher sum rates than that of the IRS-OMA scheme when the proposed manifold optimization-based algorithm is used.

II. System Model

An IRS-assisted uplink NOMA system is considered in Fig. 1 where K single antenna users send data to the base station (BS) with the assistance of an IRS panel. The IRS panel has L reflecting elements where the ith element can adjust the incident signal by adding a phase shift of θ_i upon reflection. The direct channels between the users and the BS, v_k, are considered as independent and identically distributed (i.i.d.) Rayleigh fading channels without line-of-sight (LoS) as blockages may exist between the BS and the users.

The channel vectors for IRS-BS and the kth UE-IRS paths are, respectively, denoted by $\mathbf{g} \in \mathbb{C}^{L\times 1}$ and $\mathbf{h}_k$. The IRS panel is typically placed in the area such that a strong LoS to the users and BS is obtained. Hence, a Rician channel model is considered in this paper to capture the fading coefficients of $\mathbf{g}$ and $\mathbf{h}_k$. Thus, the channel vector $\mathbf{g}$ or $\mathbf{h}_k$ can be represented as

$$\mathbf{q} = \sqrt{\frac{PL(d_q)K_q}{K_q+1}}\mathbf{q}^{LoS} + \sqrt{\frac{PL(d_q)}{K_q+1}}\mathbf{q}^{NLoS}, \tag{1}$$

where $\mathbf{q} \in \{\mathbf{g}, \mathbf{h}_k\}$, K_q is the Rician factor of the corresponding channel vector, $d_{\mathbf{g}}$ is the distance from IRS to BS, $d_{\mathbf{h}_k}$ is the distance between the kth user and the IRS, $\mathbf{q}^{LoS}$ and $\mathbf{q}^{NLoS}$ are, respectively, the LoS and non-LoS (NLoS) channel components. Since a Rician channel is considered, the LoS component is deterministic whereas the elements of $\mathbf{q}^{NLoS}$ are i.i.d. complex normal random variables $\mathcal{CN}(0,1)$. The path loss factor, PL, is given by

$$PL(d) = \eta_0 \left(\frac{d}{d_0}\right)^{-\alpha}, \tag{2}$$

where η_0 is the path loss at a reference distance of $d_0 = 1$ m, d represents the distance between transceivers, and α is the path loss exponent.

Since NOMA transmission protocol is employed, K simultaneous signals are transmitted by the K users; hence, the superimposed received signal at BS in the uplink scenario can be expressed as

$$y = \sum_{k=1}^{K}(\mathbf{g}^T\mathbf{\Theta}\mathbf{h}_k + v_k)\sqrt{p_k}s_k + n, \tag{3}$$

where s_k is the data symbol transmitted by the kth user and picked from a normalized constellation, i.e., $\mathbb{E}[|s_k|^2] = 1$, p_k is the transmitted power, and n is the complex additive white Gaussian noise (AWGN) at the BS, $\mathcal{CN}(0,\sigma_n^2)$. $\mathbf{\Theta}$ is an $L\times L$ diagonal matrix, i.e., $\mathbf{\Theta}$=diag$\{\mathbf{w}\}$, whose diagonal elements are the reflection coefficients of the IRS panel elements with $\mathbf{w}$=$[e^{j\theta_1},\ldots,e^{j\theta_L}]^T$. The angle $\theta_i \in [0,2\pi)$ represents the phase shift applied by the ith reflecting element.

In uplink NOMA systems, BS performs SIC to decode the K users' signals in a sequential manner. For efficient SIC, ordering the users according to their effective channel gains is required at the BS. Accordingly, the users with stronger channel gains are decoded first, treating the other interfering signals with weaker channel gains as noise. In the case of IRS based NOMA, the equivalent channel of the kth user is $\mathbf{g}^T\mathbf{\Theta}\mathbf{h}_k+v_k$, which indicates that the channel strength depends on $\mathbf{\Theta}$. Therefore, in this paper, the users are ordered according to the maximum achievable effective channel [24]. For example, the maximum achievable effective channel gain for the kth user can be evaluated assuming that the IRS phases are optimized such that the channel gain of this user is maximized. In this scenario, the IRS phases should be designed to align the individual channels with the phase of the direct link v_k, i.e., θ_i=$\theta_{v_k}-\theta_{g_i}-\theta_{h_{ki}}$. Therefore, the maximum achievable channel gain for user k is $\sum_{i=1}^{L}|g_i||h_{ki}|+|v_k|$, which is the value we use to order the users in the network. Without loss of generality, the users are assumed to be ordered in descending order as

$$\sum_{i=1}^{L}|g_i||h_{1i}|+|v_1| \geq \ldots \geq \sum_{i=1}^{L}|g_i||h_{Ki}|+|v_K|. \tag{4}$$

Assuming perfect SIC is applied at the BS, the decoding signal-to-interference-plus-noise-ratio (SINR) of the kth user can be expressed as

$$\gamma_k = \frac{p_k\left|\mathbf{g}^T\mathbf{\Theta}\mathbf{h}_k+v_k\right|^2}{\sum_{j=k+1}^{K}p_j\left|\mathbf{g}^T\mathbf{\Theta}\mathbf{h}_j+v_j\right|^2+\sigma_n^2}, \tag{5}$$

where $\sum_{j=k+1}^{K}p_j\left|\mathbf{g}^T\mathbf{\Theta}\mathbf{h}_j+v_j\right|^2 = 0$ when $k=K$, i.e., the Kth user does not suffer any sort of interference assuming that the previous $K-1$ signals have been successfully decoded. Consequently, the corresponding achievable rate of the kth user can be expressed as

$$R_k = \log_2(1+\gamma_k), \quad \forall k. \tag{6}$$

III. Problem Formulation and the Proposed Solution

In this section, we aim to maximize the sum throughput of the IRS-assisted uplink NOMA system. For applications

with limited power radiation or in systems where the nodes are portable and have limited batteries, each user node has a maximum transmit power constraint that cannot be exceeded. On the other hand, the system's throughput is considered a key metric in such applications, and there are quality-of-service (QoS) constraints that must be met. Therefore, in this work, we study the throughput maximization of the proposed system model while having power constraints for battery-limited users. This is done by optimizing the passive beamforming coefficients at the IRS and the transmit powers of the users to maximize the system's sum rate while having minimum rate constraints for the users to achieve fairness among them.

The sum rate of the uplink NOMA system can be re-formulated as

$$R_{\text{tot}}=\sum_{k=1}^{K}\log_2\left(1+\gamma_k\right)=\log_2\left(1+\frac{\sum_{k=1}^{K}p_k\left|\mathbf{g}^T\boldsymbol{\Theta}\mathbf{h}_k+v_k\right|^2}{\sigma_n^2}\right), \tag{7}$$

where the last identity holds because the terms inside the $\log_2$ function form a telescoping product. Since the $\log$ function is monotonically increasing, maximizing it is equivalent to maximizing the term inside. Hence, the considered sum-rate maximization problem can be formulated as

$$\max_{\mathbf{p},\boldsymbol{\Theta}} \quad \sum_{k=1}^{K}p_k\left|\mathbf{g}^T\boldsymbol{\Theta}\mathbf{h}_k+v_k\right|^2 \tag{8a}$$

$$\text{s.t.} \quad p_k\le p_k^{\max} \tag{8b}$$

$$\log_2\left(1+\frac{p_k\left|\mathbf{g}^T\boldsymbol{\Theta}\mathbf{h}_k+v_k\right|^2}{\sum_{j=k+1}^{K}p_j\left|\mathbf{g}^T\boldsymbol{\Theta}\mathbf{h}_j+v_j\right|^2+\sigma_n^2}\right)\ge R_k^{min}, \tag{8c}$$

$$k=1,2,\ldots,K,$$

$$|w_i|=1, \qquad i=1,2,\ldots,L, \tag{8d}$$

where $w_i=e^{j\theta_i}$ is the (i,i) entry of $\boldsymbol{\Theta}$, $p_k^{\max}$ is the maximum transmit power allowed at user k, and R_k^{min} is the minimum required rate. Problem (8) is non-convex since its optimization variables, p_k and w_i, are multiplied by each others. Since p_k's and w_i's are coupled together in (8), the power allocation and the IRS coefficients can be optimized alternatively using an alternating optimization technique as follows.

A. Power allocation at the users

In each iteration, for a given value of $\boldsymbol{\Theta}$, the power allocation problem in $\mathbf{p}$ reduces to

$$\max_{\mathbf{p}} \quad \sum_{k=1}^{K}p_k\left|\mathbf{g}^T\boldsymbol{\Theta}\mathbf{h}_k+v_k\right|^2 \tag{9a}$$

$$\text{s.t.} \quad p_k\le p_k^{\max} \tag{9b}$$

$$p_k\left|\mathbf{g}^T\boldsymbol{\Theta}\mathbf{h}_k+v_k\right|^2-(2^{R_k^{min}}-1)\times\left(\sum_{j=k+1}^{K}p_j\left|\mathbf{g}^T\boldsymbol{\Theta}\mathbf{h}_j+v_j\right|^2+\sigma_n^2\right)\ge 0, \quad \forall k. \tag{9c}$$

Clearly, the objective function in (9a) is linear in $\mathbf{p}$, and the constraints in (9b) and (9c) are affine inequalities. Therefore, the optimization problem in (9) is a linear program in $\mathbf{p}$, which can be easily solved using standard optimization tools.

B. Optimizing the IRS phases, $\boldsymbol{\Theta}$, using manifold optimization

In this subsection, an efficient manifold optimization-based algorithm is proposed to optimize the IRS passive beamforming vector, $\mathbf{w}$, given $\mathbf{p}$. The optimization problem in $\mathbf{w}$ can be given as

$$\max_{\mathbf{w}} \quad \sum_{k=1}^{K}p_k\left|\mathbf{d}_k^T\mathbf{w}+v_k\right|^2 \tag{10a}$$

$$\text{s.t.} \quad C_k(\mathbf{w})=p_k\left|\mathbf{d}_k^T\mathbf{w}+v_k\right|^2-(2^{R_k^{min}}-1)\times\left(\sum_{j=k+1}^{K}p_j\left|\mathbf{d}_k^T\mathbf{w}+v_j\right|^2+\sigma_n^2\right)\ge 0, \tag{10b}$$

$$k=1,2,\ldots,K,$$

$$|w_i|=1, \qquad i=1,2,\ldots,L, \tag{10c}$$

where $\mathbf{w}$ is a vector that contains the diagonal elements of $\boldsymbol{\Theta}$, and the vector $\mathbf{d}_k=\mathbf{h}_k\odot\mathbf{g}$ is the Hadamard product of the two vectors $\mathbf{h}_k$ and $\mathbf{g}$. The unit-modulus constraints on the elements of the optimization vector, $\mathbf{w}$, restrict the feasible set of the problem to lie on the surface of a smooth Riemannian manifold contained in $\mathbb{C}^L$. Specifically, each element, w_i, of the optimization vector always lies on a continuous surface called the complex circle manifold, which is a smooth Riemannian sub-manifold of $\mathbb{C}$, and it is defined as

$$\mathcal{S}=\{w_i\in\mathbb{C}:|w_i|=1\}. \tag{11}$$

Since the optimization vector, $\mathbf{w}$, in (10) contains L optimization variables, then the feasible set of (10) lies on the Cartesian product of L complex circles. This Cartesian product is also a smooth Riemannian sub-manifold of $\mathbb{C}^L$ called L-dimensional complex circle manifold, and it is defined as

$$\mathcal{S}^L\triangleq\mathcal{S}_1\times\ldots\times\mathcal{S}_L=\{\mathbf{w}=[w_1,\cdots,w_L]^T\in\mathbb{C}^L:|w_i|=1\}. \tag{12}$$

In the following, we propose how to tackle the minimum-rate constraints in (10b). By incorporating these constraints into the objective function in (10a) as penalty terms, the resulting unconstrained problem can be solved using efficient manifold optimization techniques. This approach is called the exact penalty method [25]. For each constraint, a weighted penalty term is added to the objective function in (10a). These penalty terms largely penalize the objective function if the corresponding constraints are violated. Therefore, the resultant unconstrained version of problem (10) over the L-dimensional complex circle manifold is given as

$$\max_{\mathbf{w}\in\mathcal{M}} \quad \sum_{k=1}^{K}p_k\left|\mathbf{d}_k^T\mathbf{w}+v_k\right|^2-\rho\left(\sum_{k=1}^{K}\max\{0,-C_k(\mathbf{w})\}\right), \tag{13}$$

where $\rho>0$ is a penalty weight, and $\mathcal{M}$ is the L-dimensional complex circle manifold. By solving (13) over the manifold

$\mathcal{M}$, the unit modulus constraints in (10c) are automatically satisfied.

The $\max$ functions in the unconstrained problem in (13) cause the cost function not to be smooth nor differentiable. Hence, a smooth and differentiable approximation of the $\max$ function needs to be used. The linear-quadratic loss function in [26] can be utilized to approximate the $\max$ function using a smoothing parameter $u > 0$, as $\max\{0, x\} \approx \mathcal{P}(x, u)$, where $\mathcal{P}(x, u)$ is given by

$$\mathcal{P}(x,u) = \begin{cases} 0 & x \leq 0 \\ \frac{x^2}{2u} & 0 \leq x \leq u \\ x - \frac{u}{2} & x \geq u, \end{cases} \tag{14}$$

Therefore, a smooth and differentiable version of (13) can be expressed as

$$\max_{\mathbf{w}\in\mathcal{M}} \quad Q(\mathbf{w}) = \sum_{k=1}^{K} p_k \left|\mathbf{d}_k^T\mathbf{w} + v_k\right|^2 + \rho\left(\sum_{k=1}^{K} \mathcal{P}(-C_k(\mathbf{w}), u)\right). \tag{15}$$

Now, gradient-based manifold optimization algorithms can be utilized to solve (15) over the manifold $\mathcal{M}$.

Similar to Euclidean spaces, gradient-descent optimization on Riemannian manifolds has two main steps. The first step is to find the steepest descent direction on the manifold, and the second step is to compute a step size along this direction. Repeating these two steps in each iteration allows the algorithm to converge to a local minimum point. At this point, the steepest descent direction at any point on the manifold is the *Riemannian gradient*. The Riemannian gradient at a point, $\mathbf{w}$, is the projection of the Euclidean gradient onto the tangent space, $T_{\mathbf{w}}\mathcal{M}$, at that point. The tangent space at a point, $\mathbf{w}$, on a differentiable manifold, $\mathcal{M}$, is defined as the vector space that contains all the possible directions in which one can tangentially pass through $\mathbf{w}$. The tangent space at $\mathbf{w}$ is given as

$$T_{\mathbf{w}}\mathcal{M} = \{\mathbf{v} \in \mathbb{C}^L : \Re(\mathbf{v} \odot \mathbf{w}^*) = \mathbf{0}_L\}, \tag{16}$$

where $\Re(.)$ denotes the element-wise real-part of the complex vector, and $\odot$ is the Hadamard product of two vectors. The orthogonal projection operator of a vector $\mathbf{v}$ onto the tangent space, $T_{\mathbf{w}}\mathcal{M}$, at point $\mathbf{w}$ on the manifold is given by [25]

$$P_{T_{\mathbf{w}}\mathcal{M}}(\mathbf{v}) = \mathbf{v} - \Re(\mathbf{v} \odot \mathbf{w}^*) \odot \mathbf{w}. \tag{17}$$

Therefore, the Riemannian gradient of the smooth differentiable function Q in (15) can be expressed as

$$\begin{aligned} \nabla_{\mathcal{M}} Q(\mathbf{w}) &= P_{T_{\mathbf{w}}\mathcal{M}}(\nabla Q(\mathbf{w})) \\ &= \nabla Q(\mathbf{w}) - \Re(\nabla Q(\mathbf{w}) \odot \mathbf{w}^*) \odot \mathbf{w}, \end{aligned} \tag{18}$$

where $\nabla Q(\mathbf{w})$ is the Euclidean gradient at the point $\mathbf{w}$. In the following, we derive the Euclidean gradient of Q; the Euclidean gradient is given by

$$\nabla Q(\mathbf{w}) = \left[\frac{\partial Q}{\partial w_1} \; \frac{\partial Q}{\partial w_2} \cdots \frac{\partial Q}{\partial w_L}\right]^T, \tag{19}$$

where $\partial Q/\partial w_i = \partial Q/\partial \Re(w_i) + j\partial Q/\partial \Im(w_i)$, and $\Im(.)$ denotes the imaginary part of a complex number. The partial derivative w.r.t. w_i can be calculated as

$$\frac{\partial Q}{\partial w_i} = \frac{\partial f}{\partial w_i} + \rho \sum_{k=1}^{K} \frac{\partial}{\partial w_i} \mathcal{P}(-C_k(\mathbf{w}), u), \tag{20}$$

where f is the first term of the objective function Q in (15). The partial derivative of f w.r.t. w_i can be derived as

$$\begin{aligned} \frac{\partial f}{\partial w_i} &= \frac{\partial f}{\partial \Re(w_i)} + j\frac{\partial f}{\partial \Im(w_i)} \\ &= \sum_{k=1}^{K} p_k \Big(2\Re(\mathbf{d}_k^T\mathbf{\Theta})(a_{ki} - jb_{ki}) + 2\Im(\mathbf{d}_k^T\mathbf{\Theta})(b_{ki} + ja_{ki})\Big), \end{aligned} \tag{21}$$

where $a_{ki} = \Re(h_{ki}g_i)$, $b_{ki} = \Im(h_{ki}g_i)$. The partial derivative, $\frac{\partial \mathcal{P}(-C_k(\mathbf{\Theta}), u)}{\partial w_i}$, is calculated as

$$\frac{\partial \mathcal{P}(-C_k(\mathbf{\Theta}), u)}{\partial w_i} = \begin{cases} 0 & -C_k(\mathbf{\Theta}, u) \leq 0 \\ \frac{C_k(\mathbf{\Theta})}{u} C'_{ki}(\mathbf{\Theta}) & 0 \leq -C_k(\mathbf{\Theta}, u) \leq u \\ -C'_{ki}(\mathbf{\Theta}) & -C_k(\mathbf{\Theta}, u) \geq u, \end{cases} \tag{22}$$

where $C'_{ki}(\mathbf{\Theta})$ is derived as

$$\begin{aligned} C'_{ki}(\mathbf{\Theta}) &= \frac{\partial C_k(\mathbf{\Theta})}{\partial \Re(w_i)} + j\frac{\partial C_k(\mathbf{\Theta})}{\partial \Im(w_i)} \\ &= p_k \Big(2\Re(\mathbf{d}_k^T\mathbf{\Theta})(a_{ki} - jb_{ki}) + 2\Im(\mathbf{d}_k^T\mathbf{\Theta})(b_{ki} + ja_{ki})\Big) \\ &\quad - (2^{R_k^{min}} - 1)\Big\{ \sum_{l=k+1}^{K} p_l \Big(2\Re(\mathbf{d}_k^T\mathbf{\Theta})(a_{li} - jb_{li}) \\ &\quad + 2\Im(\mathbf{d}_k^T\mathbf{\Theta})(b_{li} + ja_{li})\Big)\Big\}. \end{aligned} \tag{23}$$

Then, by substituting (21) and (22) in (20), we obtain the Euclidean gradient, which is required to calculate the Riemannian gradient in (18) for our algorithm. **Algorithm 1** shows the procedures of solving the penalized manifold optimization problem in (15) and how the penalty coefficient ρ and the smoothing parameter u are properly chosen iteratively.

The behavior of **Algorithm 1** is explained here by emphasizing how the parameters ρ and u are updated in each iteration. The optimum points of the penalized problem in (15) coincide with the optimum points of the original problem in (10) when ρ is above a certain threshold [25]. An iterative approach in [27] is utilized in **Algorithm 1** to find ρ since the threshold is usually unknown. **Algorithm 1** starts with a small initial value of ρ_0. Afterwards, ρ is increased in each iteration by multiplying it by $\beta_\rho > 1$ if the constraints in (10b) are violated as shown in lines 8 and 9 in **Algorithm 1**. The parameter τ is a tolerance factor which is a small positive number.

Moreover, **Algorithm 1** starts with an initial smoothing parameter u_0, then its value is decreased in each iteration by the multiplication by the fraction β_u till it reaches a minimum value $u_{\min}$. This is done to improve the accuracy of the approximation function in (22) while avoiding any numerical

Algorithm 1: Exact penalty method via smoothing

1 **Input:** Starting point $\mathbf{w}_0$, starting penalty coefficient ρ_0, starting smoothing accuracy u_0, minimum smoothing accuracy $u_{\min}$, constants $\beta_u \in (0,1)$, $\beta_\rho > 1$, $\tau \geq 0$, minimum step length $d_{\min}$.

2 **for** $l = 0, 1, 2, \ldots$ **do**

3 To obtain $\mathbf{w}_{l+1}$, choose any sub-solver to approximately solve

$$\min_{\mathbf{w}\in\mathcal{M}} \quad Q(\mathbf{w}, \rho_l, u_l)$$

with warm-start at $\mathbf{w}_l$ and stopping criterion

$$\|\text{grad } Q(\mathbf{w}, \rho_l, u_l)\| \leq \delta.$$

4 **if** $(\text{dist}(\mathbf{w}_l, \mathbf{w}_{l+1}) < d_{\min}$ or $u_l \leq u_{\min})$ and $C_k(\mathbf{w}_{l+1}) < \tau$ **then**

5 Return $\mathbf{w}_{l+1}$;

6 **end**

7 $u_{l+1} = \max\{u_{\min}, \beta_u u_l\}$;

8 **if** $(l = 0$ or $-C_k(\mathbf{w}_{l+1}) \geq \tau)$ **then**

9 $\rho_{l+1} = \beta_\rho \rho_l$

10 **else**

11 $\rho_{l+1} = \rho_l$;

12 **end**

13 **end**

inaccuracies that might arise when the smoothing parameter is too small. The manifold optimization sub-problem in line 3 is solved in each iteration using the *Manopt* MATLAB toolbox [28].

IV. Comparison with optimized IRS-assisted OMA

In this section, we discuss the baseline IRS-assisted uplink OMA scenario to compare against NOMA. An optimal solution is derived that maximizes the average sum rate of the OMA users. Unlike the NOMA scheme, in the IRS-assisted OMA, each user transmits its data separately within its allocated time fraction, α_k, while other users remain idle. This time allocation for the users, α_k's, is optimized to maximize the sum rate of the users. Since the objective is to maximize the sum rate, each user must transmit using its maximum power, $p_k^{\max}$, during its allocated time to maximize its rate, hence, maximizing the sum rate. Therefore, the optimization problem can be expressed as

$$\max_{\alpha_k, \boldsymbol{\Theta}_k} \quad \sum_{k=1}^{K} \alpha_k \log_2\left(1 + \frac{p_k^{\max}|\mathbf{g}^T\boldsymbol{\Theta}_k\mathbf{h}_k + v_k|^2}{\sigma_n^2}\right) \tag{24a}$$

$$\text{s.t.} \quad \alpha_k \log_2\left(1 + \frac{p_k^{\max}|\mathbf{g}^T\boldsymbol{\Theta}_k\mathbf{h}_k + v_k|^2}{\sigma_n^2}\right) \geq R_k^{min}, \quad \forall k, \tag{24b}$$

$$\sum_{k=1}^{K} \alpha_k = 1. \tag{24c}$$

Since in OMA each user transmits its data separately within its allocated time, the optimization of the passive beamforming at the IRS can be performed separately for each user. The IRS phase shifts are chosen so that all the elements of the cascaded user-IRS-BS channel, $h_{ki}w_i g_i \forall i$, are aligned to have the same phase, which is the phase of the direct channel v_k, i.e., $\theta_i = \theta_{v_k} - \theta_{g_i} - \theta_{h_{ki}}$. This way, each user can maximize its effective channel gain, which maximizes the sum rate. By substituting the values of $\boldsymbol{\Theta}_k$ in (24) and solving the linear program in α_k, we can readily get the optimal OMA time allocation for each user.

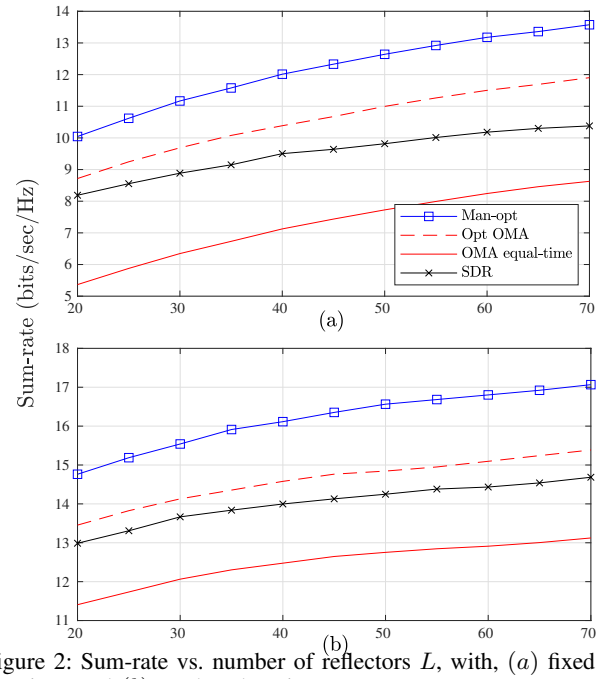

Figure 2: Sum-rate vs. number of reflectors L, with, (a) fixed locations and (b) random locations

V. Simulation Results

In this section, we provide extensive simulation results to validate the proposed manifold optimization-based algorithm for IRS-assisted uplink NOMA system. The results of the proposed algorithm are compared against the results of the SDR-based optimization as a benchmark because SDR is widely used in the IRS optimization literature. Additionally, the IRS-assisted NOMA system is compared against the IRS-assisted OMA baseline to demonstrate the superiority of NOMA over OMA in the considered simulation scenarios.

The following are the simulation parameters used [29]. The path loss at the reference distance in (2) is set to be $\eta_0 = 10^{-3}$, and the path loss exponents for the direct links (users to BS), IRS to users links and BS to IRS link are assumed in this simulation setup to be $\alpha_{BU} = 5.5$, $\alpha_{IU} = 2.2$ and $\alpha_{BI} = 2.2$, respectively. The noise power σ_n^2 is set to be -114 dBm, and the Rician factor of the channels in (1) is set as $K_q = 2.2$. The number of users is set as $K = 3$, whereas the maximum transmission power allowed at each user is 20 mW. All the simulation results are averaged over 10^3 trials.

Fig. 2 shows the sum rate performance for different scenarios versus the number of IRS reflecting elements, L. In Fig. 2 (a), the locations of the IRS and the users are assumed static where the IRS-users distances are set to be $\{10, 40, 100\}$

m, the BS-IRS distance is 25 m, and the BS-users distances are set to be $\{30, 80, 200\}$ m, respectively. Whereas in Fig. 2 (b), the BS-IRS and the IRS-users distances are randomly, uniformly-generated within the interval between 50 m and 100 m. Then, in each trial, the users are ordered according to their effective channel strength as in (4), and the performance is averaged over all trials.

The figure shows that the performance of the proposed manifold optimization algorithm is superior to the SDR-based solution, which is widely used in the literature. The figure also reveals that the manifold optimization based NOMA outperforms both optimized and equal-time (i.e., $\alpha_k = 1/K$) OMA schemes. This is expected since there are large differences between the users' distances to the IRS which is the NOMA-favorable situation. However, the graph shows that the NOMA-SDR can only beat the equal-time OMA, but results in inferior performance compared to the optimized OMA scenario. This observation signifies the importance of the proposed manifold optimization technique to achieve the IRS-NOMA expected gains, especially, in the NOMA favorable scenarios.

VI. Conclusions

This paper proposes an efficient manifold-based optimization technique for the passive beamforming problem at the IRS in the context of uplink NOMA transmission. The proposed algorithm significantly outperforms the SDR-based optimization technique. Simulation results show that the SDR-based technique cannot outperform the optimized OMA scheme in the simulated scenarios. This is because SDR is not well-suited to tune the IRS phases to achieve the full gains of IRS-NOMA scheme. However, the proposed IRS-NOMA manifold-based optimization technique can reap the gains of the IRS-NOMA scheme and show its superiority in the scenarios where IRS-NOMA is expected to do better than the IRS-OMA schemes.

Acknowledgement

This work was supported by the European Union's Horizon 2020 Research and Innovation Program through the Marie Sklodowska-Curie under grant agreement number 812991.

References

[1] N. Babu, C. B. Papadias, and P. Popovski, "Energy-efficient 3-D deployment of aerial access points in a UAV communication system," *IEEE Commun. Lett.*, vol. 24, no. 12, pp. 2883-2887, Dec. 2020.

[2] X. Jing, J. Sun, and C. Masouros, "Energy aware trajectory optimization for aerial base stations," *IEEE Trans. Commun.*, vol. 69, no. 5, pp. 3352-3366, May 2021.

[3] H. Azarhava and J. Musevi Niya, "Energy efficient resource allocation in wireless energy harvesting sensor networks," *IEEE Wireless Commun. Lett.*, vol. 9, no. 7, pp. 1000-1003, Jul. 2020.

[4] K. Wang, H. Gao, X. Xu, J. Jiang, and D. Yue, "An energy-efficient reliable data transmission scheme for complex environmental monitoring in underwater acoustic sensor networks," *IEEE Sensors J.*, vol. 16, no. 11, pp. 4051-4062, Jun. 2016

[5] M. Ahmad, N. Al-ababneh, and M. Al-Ibrahim, "Cooperative OFDM for semi distributed detection in wireless sensor networks," *AEU-Int. J. Electron. Commun.*, vol. 68, no. 10, pp. 1022-1029, 2014.

[6] M. A. Al-Jarrah, M. A. Yaseen, A. Al-Dweik, O. A. Dobre, and E. Alsusa, "Decision Fusion for IoT-Based Wireless Sensor Networks," *IEEE IoT J.*, vol. 7, no. 2, pp. 1313-1326, Feb. 2020.

[7] E. Basar, M. Di Renzo, J. De Rosny, M. Debbah, M.-S. Alouini, and R. Zhang, "Wireless communications through reconfigurable intelligent surfaces," *IEEE Access*, vol. 7, pp. 116753-116773, 2019.

[8] M. Al-Jarrah, A. Al-Dweik, E. Alsusa, and M.-S. Alouni, "Performance analysis of wireless mesh backhauling using intelligent reflecting surface," *IEEE Trans. Wireless Commun.*, vol. 20, no. 6, pp. 3597-3610, 2021.

[9] M. A. ElMossallamy, H. Zhang, L. Song, K. G. Seddik, Z. Han, and G. Y. Li, "Reconfigurable intelligent surfaces for wireless communications: Principles, challenges, and opportunities, " *IEEE Trans. Cognitive Commun. Netw.*, vol. 6, no. 3, pp. 990–1002, 2020.

[10] M. A. ElMossallamy, H. Zhang, R. Sultan, K. G. Seddik, L. Song, G. Y. Li, and Z. Han, "On spatial multiplexing using reconfigurable intelligent surfaces, " *IEEE Wireless Commun. Lett.*, vol. 10, no. 2, pp. 226–230, 2021.

[11] M. Al-Jarrah, A. Al-Dweik, E. Alsusa, Y. Iraqi, and M.-S. Alouini, "IRS-assisted UAV communications with imperfect phase compensation," *IEEE Trans. Commun.*, vol. 69, no. 12, pp. 8551-8568, 2021.

[12] M. Al-Jarrah, E. Alsusa, A. Al-Dweik, and Daniel K. C. So, "Capacity analysis of IRS-based UAV communications with imperfect phase compensation," *IEEE Wireless Commun. Lett.*, vol. 10, no. 10, pp. 1479-1483, Jul. 2021.

[13] K. G. Seddik, "On the degrees of freedom of IRS-assisted non-Coherent MIMO communications, " *IEEE Commun. Lett.*, vol. 26, no. 5, pp. 1175-1179, May 2022, doi: 10.1109/LCOMM.2022.3153556.

[14] T. Assaf *et al.*, "NOMA receiver design for delay-sensitive systems," *IEEE Systems J.*, vol. 15, no. 4, pp. 5606-5617, 2021.

[15] F. Fang, Y. Xu, Q.-V. Pham, and Z. Ding, "Energy-efficient design of IRS-NOMA networks," *IEEE Trans. Vehic. Technol.*, vol. 69, no. 11, pp. 14088-14092, Nov. 2020.

[16] J. Zhu, Y. Huang, J. Wang, K. Navaie, and Z. Ding, "Power efficient IRS-assisted NOMA," *IEEE Trans. Commun.*, vol. 69, no. 2, pp. 900-913, Feb. 2021.

[17] Z. Sun and Y. Jing, "On the performance of multi-antenna IRS-assisted NOMA networks with continuous and discrete IRS phase shifting," *IEEE Trans. Wireless Commun.*, IEEE early access, doi: 10.1109/TWC.2021.3117494.

[18] M. Zeng, X. Li, G. Li, W. Hao, and O. A. Dobre, "Sum rate maximization for IRS-assisted uplink NOMA," *IEEE Commun. Lett.*, vol. 25, no. 1, pp. 234-238, Jan. 2021.

[19] B. Lyu, P. Ramezani, D. T. Hoang, and A. Jamalipour, "IRS-Assisted Downlink and Uplink NOMA in Wireless Powered Communication Networks," *IEEE Trans. Vehic. Technol.*, vol. 71, no. 1, pp. 1083-1088, Jan. 2022.

[20] B. Tahir, S. Schwarz, M. Rupp, "Outage analysis of uplink IRS-assisted NOMA under elements splitting," *2021 IEEE 93rd Vehic. Technol. Conf. (VTC2021-Spring)*, 2021, pp. 1-5.

[21] M. A. ElMossallamy, K. G. Seddik, W. Chen, L. Wang, G. Y. Li and Z. Han, "RIS optimization on the complex circle manifold for interference mitigation in interference channels, " *IEEE Trans. Vehic. Technol.*, vol. 70, no. 6, pp. 6184-6189, Jun. 2021.

[22] M. Alaaeldin, E. A. Alsusa, and K. G. Seddik, "IRS-assisted physical layer network coding over two-way relay fading channels," *IEEE Trans. Veh. Technol.*, pp. 1–1, 2022.

[23] M. AlaaEldin, E. Alsusa, K. G. Seddik, C. B. Papadias, and M. Al-Jarrah, "Optimization of energy-constrained IRS-NOMA using a complex circle manifold approach," *Arxiv Preprint*, [Online]. Available: https://arxiv.org/abs/2206.01312.

[24] G. Yang, X. Xu and Y. -C. Liang, "Intelligent reflecting surface assisted non-orthogonal multiple access," *2020 IEEE Wireless Commun. Netw. Conf. (WCNC)*, 2020, pp. 1-6.

[25] P.-A. Absil, R. Mahony, and R. Sepulchre, "Optimization algorithms on matrix manifolds," *Princeton, NJ: Princeton University Press*, 2008.

[26] M. C. Pinar and S. A. Zenios, "On smoothing exact penalty functions for convex constrained optimization," *SIAM J. Optimization*, vol. 4, no. 3, 1994.

[27] C. Liu and N. Boumal, "Simple algorithms for optimization on Riemannian manifolds with constraints," *Appl Math Optim*, vol. 82, no. 3, pp. 949–981, 2020.

[28] N. Boumal, B. Mishra, P.-A. Absil, and R. Sepulchre, "Manopt, a MATLAB toolbox for optimization on manifolds," *J. Machine Learning Research*, vol. 15, no. 42, pp. 1455–1459, 2014. [Online]. Available: https://www.manopt.org

[29] Q. Wu and R. Zhang, "Intelligent reflecting surface enhanced wireless network via joint active and passive beamforming," *IEEE Trans. Wireless Commun.*, vol. 18, no. 11, pp. 5394–5409, 2019.